

# $^{64}\text{Cu}$ -TETA-Octreotide as a PET Imaging Agent for Patients with Neuroendocrine Tumors

Carolyn J. Anderson, Farrokh Dehdashti, P. Duffy Cutler, Sally W. Schwarz, Richard Laforest, Laura A. Bass, Jason S. Lewis, and Deborah W. McCarthy

Mallinckrodt Institute of Radiology, Washington University School of Medicine, St. Louis, Missouri

$^{64}\text{Cu}$  (half-life, 12.7 h;  $\beta^+$ , 0.653 MeV [17.4%];  $\beta^-$ , 0.579 MeV [39%]) has shown potential as a radioisotope for PET imaging and radiotherapy.  $^{111}\text{In}$ -diethylenetriaminepentaacetic acid (DTPA)-D-Phe<sup>1</sup>-octreotide (OC) was developed for imaging somatostatin-receptor-positive tumors using conventional scintigraphy. With the advantages of PET over conventional scintigraphy, an agent for PET imaging of these tumors is desirable. Here, we show that  $^{64}\text{Cu}$ -TETA-OC (where TETA is 1,4,8,11-tetraazacyclotetradecane-*N,N',N'',N'''*-tetraacetic acid) and PET can be used to detect somatostatin-receptor-positive tumors in humans. **Methods:** Eight patients with a history of neuroendocrine tumors (five patients with carcinoid tumors and three patients with islet cell tumors) were imaged by conventional scintigraphy with  $^{111}\text{In}$ -DTPA-OC (204–233 MBq [5.5–6.3 mCi]) and by PET imaging with  $^{64}\text{Cu}$ -TETA-OC (111 MBq [3 mCi]). Blood and urine samples were collected for pharmacokinetic analysis. PET images were collected at times ranging from 0 to 36 h after injection, and the absorbed doses to normal organs were determined. **Results:** In six of the eight patients, cancerous lesions were visible by both  $^{111}\text{In}$ -DTPA-OC SPECT and  $^{64}\text{Cu}$ -TETA-OC PET. In one patient,  $^{111}\text{In}$ -DTPA-OC showed mild uptake in a lung lesion that was not detected by  $^{64}\text{Cu}$ -TETA-OC PET. In one patient, no tumors were detected by either agent; however, pathologic follow-up indicated that the patient had no tumors. In two patients whose tumors were visualized with  $^{111}\text{In}$ -DTPA-OC and  $^{64}\text{Cu}$ -TETA-OC,  $^{64}\text{Cu}$ -TETA-OC and PET showed more lesions than  $^{111}\text{In}$ -DTPA-OC. Pharmacokinetic studies showed that  $^{64}\text{Cu}$ -TETA-OC was rapidly cleared from the blood and that  $59.2\% \pm 17.6\%$  of the injected dose was excreted in the urine. Absorbed dose measurements indicated that the bladder wall was the dose-limiting organ. **Conclusion:** The high rate of lesion detection, sensitivity, and favorable dosimetry and pharmacokinetics of  $^{64}\text{Cu}$ -TETA-OC indicate that it is a promising radiopharmaceutical for PET imaging of patients with neuroendocrine tumors.

**Key Words:**  $^{64}\text{Cu}$ ; octreotide; PET;  $^{111}\text{In}$

**J Nucl Med 2001; 42:213–221**

**T**argeting of somatostatin receptors (SSRs) in tumors has been a goal in cancer treatment and diagnosis since the 1980s. The somatostatin analog octreotide (OC) has been labeled with  $^{123}\text{I}$  (1) and  $^{111}\text{In}$  (2) and used to image SSR-positive tumors in humans (3) by conventional scintigraphy.  $^{123}\text{I}$ -Tyr<sup>3</sup>-OC has a high hepatobiliary excretion that hinders visualization of tumors in the abdomen, whereas  $^{111}\text{In}$ -diethylenetriaminepentaacetic acid (DTPA)-D-Phe<sup>1</sup>-OC clears primarily through the kidneys (3) and is currently used routinely as an imaging agent for neuroendocrine tumors. Because of the limited sensitivity and resolution of SPECT, we are interested in designing a positron-emitting agent for PET imaging of SSR-positive tumors. Using OC labeled with a positron-emitting radionuclide and PET, tracer accumulation within tissues can be quantitatively assessed, potentially offering improvements over SPECT when quantitative results are needed and when tumors are small or deep within the body.

An attractive radionuclide for PET imaging is  $^{64}\text{Cu}$  (half-life, 12.7 h; 39%  $\beta^-$  [0.579 MeV]; 17.4%  $\beta^+$  [0.653 MeV]; 43.6% electron capture).  $^{64}\text{Cu}$  can be produced by either a reactor (4) or a medical cyclotron (5). Recently, a method was developed at Washington University School of Medicine to produce large quantities of  $^{64}\text{Cu}$  (up to 37 GBq) on demand using a biomedical cyclotron (5).  $^{64}\text{Cu}$  also has shown potential as a therapeutic radionuclide. In radioimmunotherapy studies, we showed that  $^{64}\text{Cu}$ -labeled monoclonal antibody 1A3 caused complete tumor regression with no regrowth of tumors in a well-established animal model (6,7).

We showed that  $^{64}\text{Cu}$ -TETA-OC (where TETA is 1,4,8,11-tetraazacyclotetradecane-*N,N',N'',N'''*-tetraacetic acid) had a similar biodistribution to  $^{111}\text{In}$ -DTPA-OC in a tumor-bearing rat model (8). In targeted radiotherapy studies,  $^{64}\text{Cu}$ -TETA-OC inhibited the growth of tumors in the same tumor-bearing rat model (9). PET imaging of tumors using low doses of  $^{64}\text{Cu}$ -TETA-OC could also be used to determine individual absorbed doses before therapy with either  $^{64}\text{Cu}$ - or  $^{67}\text{Cu}$ -labeled OC. For these reasons, we are investigating  $^{64}\text{Cu}$ -TETA-OC as a PET imaging agent for patients with neuroendocrine tumors.

In this study, we compared  $^{64}\text{Cu}$ -TETA-OC and PET with  $^{111}\text{In}$ -DTPA-OC and conventional scintigraphy in

Received Apr. 6, 2000; revision accepted Aug. 14, 2000.

For correspondence or reprints contact: Carolyn J. Anderson, PhD, Mallinckrodt Institute of Radiology, Washington University School of Medicine, 510 S. Kingshighway Blvd., Campus Box 8225, St. Louis, MO 63110.

eight patients with a history of neuroendocrine tumors. The blood and urine clearance of  $^{64}\text{Cu}$ -TETA-OC was determined, and absorbed doses to normal organs were measured from the PET images.

## MATERIALS AND METHODS

### Preparation of $^{64}\text{Cu}$ -TETA-OC

$^{64}\text{Cu}$ -TETA-OC was prepared in compliance with guidelines established by the Washington University Radioactive Drug Research Committee.  $^{64}\text{Cu}$  was produced on a biomedical cyclotron (5). The specific activity of  $^{64}\text{Cu}$  ranged from 222,000 to 1,850,000 GBq/mmol. TETA-OC was prepared as previously described (9).  $^{64}\text{Cu}$  was labeled to TETA-OC as previously described (8). Briefly,  $^{64}\text{Cu}$ -acetate (370 MBq [10 mCi]) was labeled to 10  $\mu\text{g}$  TETA-OC in 0.1 mol/L ammonium acetate buffer, pH 5.5. Gentisic acid (1 mg) was added to the radiolabeled conjugates to reduce the effects of radiolysis. The preparations were purified by a  $\text{C}_{18}$  SepPak (Waters, Milford, MA) to remove uncomplexed  $^{64}\text{Cu}$ -acetate.  $^{64}\text{Cu}$ -TETA-OC was sterile filtered with a 0.22- $\mu\text{m}$  Millex GV (Millipore, Bedford, MA) before injection. Radiochemical purity was assessed by radio-thin-layer chromatography (Bioscan, Inc., Washington, DC), using reversed-phase  $\text{C}_{18}$  plates developed in 70:30 methanol:5% ammonium acetate, and by reversed-phase high-performance liquid chromatography (Waters). Patients received an injection of 107–130 MBq (2.9–3.5 mCi) (3–5  $\mu\text{g}$ )  $^{64}\text{Cu}$ -TETA-OC.

$^{111}\text{In}$ -DTPA-OC was prepared using the OctreoScan kit provided by the manufacturer (Mallinckrodt, Inc., St. Louis, MO). Patients received an injection of 204–233 MBq (5.5–6.3 mCi)  $^{111}\text{In}$ -DTPA-OC labeled to 10  $\mu\text{g}$  DTPA-OC.

### Patients

Patients who were scheduled for routine imaging with  $^{111}\text{In}$ -DTPA-OC were eligible for  $^{64}\text{Cu}$ -TETA-OC and PET. Eight patients (six men, two women; age range, 45–70 y) with a history of neuroendocrine tumors who were being evaluated with  $^{111}\text{In}$ -DTPA-OC as part of their routine clinical evaluation also underwent PET with  $^{64}\text{Cu}$ -TETA-OC at our institution. This investigation was approved by the Human Studies Committee and the Radioactive Drug Research Committee at Washington University School of Medicine. Each patient gave informed consent before participating in the study. In all patients but one, the  $^{111}\text{In}$ -DTPA-OC was administered before  $^{64}\text{Cu}$ -TETA-OC. The time between administration of  $^{111}\text{In}$ -DTPA-OC and  $^{64}\text{Cu}$ -TETA-OC ranged from –1 to 40 d (mean time, 14 d).

### Imaging

PET imaging was performed with an ECAT EXACT scanner (Siemens/CTI, Knoxville, TN). Single-photon imaging was also performed on each patient using a dual-head Genesys scanner (ADAC Laboratories, Milpitas, CA) fitted with medium-energy collimators. Conventional scintigraphy was performed after injection of 204–233 MBq (5.5–6.3 mCi)  $^{111}\text{In}$ -DTPA-OC. All patients underwent whole-body planar scintigraphy at 4 and 24 h. The whole-body planar study consisted of anterior and posterior views proceeding from head to toe at 6 cm/min. All but one patient underwent SPECT (imaging of the chest and abdomen at 24 h in one patient and at 4 and 24 h in one patient; imaging of only the abdomen at 24 h in two patients, at 4 h in one patient, and at 4 and 24 h in two patients). Full-field SPECT was performed without

attenuation correction on the chest and abdomen for 20 min each. On a separate day, PET was performed after intravenous injection of approximately 111 MBq (3.0 mCi)  $^{64}\text{Cu}$ -TETA-OC in an antecubital vein. Delay intervals ranging from 0 to 24 h between injection and imaging were evaluated, from which an optimal delay of 4–5 h was selected as providing the best combination of image quality and lesion-to-background contrast. Five of the eight PET studies were performed to estimate the radiation dosimetry of  $^{64}\text{Cu}$ -TETA-OC. In these patients, the entire torso was scanned to allow complete determination of the activity biodistribution throughout the body. In the other three patients, only a single bed position was used, covering 16 cm axially around the suspected tumor region. At each bed position, the study consisted of static (if delayed) or dynamic (if at injection) data acquisition, 20 min in duration, followed by a 2- to 3-min transmission scan. From the transmission scan, segmented attenuation maps were derived (10) and used to apply full attenuation correction to the emission image volume. PET and SPECT images were reconstructed using filtered backprojection (Hanning filter, cutoff of 0.8 Nyquist) and were volume rendered for cinegraphic viewing.

The  $^{111}\text{In}$ -DTPA-OC and  $^{64}\text{Cu}$ -TETA-OC images were examined qualitatively. The criteria for interpretation were those routinely used in scintigraphic imaging. The PET images were examined by a nuclear medicine physician, and the interpretation of the images was based on knowledge of normal biodistribution of  $^{64}\text{Cu}$ -TETA-OC derived from animal models. Foci of abnormal radiotracer uptake were recorded on a four-point scale (0 = no uptake; + = mild uptake; ++ = moderate uptake; and +++ = intense uptake).

### Measurement of $^{64}\text{Cu}$ Activity in Blood and Urine of Patients

$^{64}\text{Cu}$  activity in the blood and urine was measured in a gamma counter (Beckman, Arlington Heights, IL) containing a NaI crystal. Two blood samples were drawn per patient at times ranging from 1.5 to 22 h after injection of  $^{64}\text{Cu}$ -TETA-OC. Urine was collected from patients (from two to six samples per patient) at times ranging from 1.5 to 27 h after injection.

### Human Absorbed Dose Measurements from Patient PET Images

For evaluation of biodistribution and calculation of dosimetry, five of the eight PET studies involved imaging the chest and abdomen at different times (0 and 4 h in two patients, 5 and 24 h in two patients, and 5 h in one patient) after administration of  $^{64}\text{Cu}$ -TETA-OC. All but one of the patients were imaged twice.

Activity was observed mainly in the liver, spleen, kidneys, bladder, and tumors. Regions of interest (ROIs) were drawn on the PET images of the five dosimetry study patients to measure the total activity in these organs. For the liver, the average activity concentration was calculated from ROIs traced inside and encompassing most of the organ for five to six adjacent slices. The average activity concentration in the liver was then multiplied by the estimated liver volume. For the other visible organs, ROIs were drawn around the entire organ. The total activity in these organs was thus directly measured. In addition, ROIs were traced around the heart to evaluate the activity concentration in the blood. The blood activity concentration was measured by the average maximum value in the slices containing the lower left ventricle. Finally, elliptic ROIs were drawn in several adjacent slices of the lower abdomen beside the bladder to measure the average soft-tissue activity concentration. The red marrow activity concentration,  $A_{\text{rm}}$ ,

was calculated from the blood activity concentration,  $A_{bl}$ , in proportion to the mass of the red marrow,  $m_{rm}$ , and assuming a hematocrit value of 39%, as follows (11):  $A_{rm} = A_{bl}m_{rm}0.19/(1 - 0.39)$ .

Measurements were repeated for each time point. The percentage of injected activity in each organ immediately after the injection (at  $t_0^+$ ) was calculated from its estimated blood volume. This decision was based on the assumption that the bolus of activity distributes uniformly throughout the body immediately after the injection. The fractions of injected activity at  $t_0^+$  were 4.9% for the liver, 5.9% for the lungs, 1.5% for the spleen, 1.4% for the kidneys, 3.7% for the bones, and 10% for the heart.

A time–activity curve was drawn for each organ combining the data from all patients. The measured organ activities were corrected for decay to the time of the start of the scan to simplify the subsequent fitting procedure. The time–activity curves were fitted with a sum of one or two exponentials in which the parameters were determined by a least squares minimization procedure. The fitted functions were then integrated analytically (including physical decay) to give the residence times. Dose calculation was performed by the MIRD methodology in which the S values were calculated with the MIRDOSE3.0 program using the adult male model. Along with any unaccounted activity, the soft-tissue activity and 72% of the blood activity were assigned to the remainder of the body as a MIRD source organ. Although some activity was seen to accumulate in the tumors, this contribution could not be included under the MIRD scheme. Instead, the tumor activity was assumed to be distributed uniformly throughout the body. An uptake function was fitted to the time-cumulated urine data from all patients. The absorbed fraction and the filling half-time were used in the MIRDOSE3 bladder model (12) along with a voiding period of 4 h to obtain the residence time of the bladder contents.

#### Human Absorbed Dose Estimates from Baboon PET Images

The biodistribution of  $^{64}\text{Cu}$ -TETA-OC was also determined in a 25-kg male baboon by PET imaging. This study was performed in

compliance with the Guidelines for the Care and Use of Research Animals established by the Animal Studies Committee of Washington University School of Medicine. Images of the animal's torso were acquired at approximately 30-min intervals from 0 to 3 h and then again at 24 h after injection. The baboon was anesthetized with isoflurane during the first 3-h imaging session and then was allowed to recover. The baboon was placed in approximately the same position the following day, anesthetized with isoflurane, and imaged for 30 min. Activity concentration values were derived from the PET images as previously described (13). The absorbed fraction and filling half-time were used in the MIRDOSE3 bladder model (12) along with a voiding period of 4 h to obtain the residence time of the bladder contents.

Blood samples were collected from the baboon at 6, 20, 40, 60, and 120 min after injection of  $^{64}\text{Cu}$ -TETA-OC. The percentage injection dose (%ID) in the blood at those times was determined, and the data were used to determine blood clearance.

## RESULTS

### Radiochemistry

$^{64}\text{Cu}$ -TETA-OC was prepared in greater than 95% radiochemical purity as shown by radio–thin-layer chromatography and radio–high-performance liquid chromatography.

### Absorbed Dose Estimates from Baboon Imaging

PET imaging of a nonhuman primate was performed to estimate the human absorbed doses before beginning human PET imaging studies. The estimated human absorbed doses from the baboon PET images, in comparison with estimated human absorbed doses from rat biodistribution data (9), are listed in Table 1. The baboon PET data suggest that the dose-limiting organ is the bladder wall (0.17 mGy/MBq [0.62 rad/mCi]), followed by the kidneys (0.13 mGy/MBq [0.49 rad/mCi]). The largest discrepancy between dosimetry

**TABLE 1**  
Estimated Human Absorbed Doses of  $^{64}\text{Cu}$ -TETA-OC to Normal Organs Using Biodistribution Data from Rats and PET Data from Baboons and Humans

Tissue	Rat* biodistribution (rad/mCi [mGy/MBq])	PET	
		Baboon (rad/mCi [mGy/MBq])	Human (rad/mCi [mGy/MBq])
Bladder wall	1.12 (0.30) <sup>†</sup>	0.62 (0.17) <sup>‡</sup>	0.94 (0.25) <sup>‡</sup> 0.23 (0.062) <sup>§</sup>
LLI wall	0.86 (0.23)	0.08 (0.021)	0.05 (0.013)
Kidneys	0.54 (0.15)	0.49 (0.13)	0.29 (0.078)
Adrenals	0.37 (0.10)	0.10 (0.027)	0.05 (0.015)
ULI wall	0.16 (0.043)	0.07 (0.020)	0.04 (0.012)
Pancreas	0.12 (0.032)	0.10 (0.027)	0.01 (0.027)
Liver	0.10 (0.027)	0.14 (0.039)	0.34 (0.091)
Marrow	0.07 (0.019)	0.07 (0.019)	0.05 (0.013)
Spleen	0.05 (0.013)	0.03 (0.0081)	0.26 (0.071)
Total body	0.10 (0.027)	0.07 (0.019)	0.05 (0.013)

\*CA20948 tumor-bearing Lewis rats (9).

<sup>†</sup>Assuming voids at 2 and 5.5 h.

<sup>‡</sup>MIRDOSE3 dynamic bladder model with void at 4 h.

<sup>§</sup>MIRDOSE3 dynamic bladder model with void at 1 h.

LLI = lower large intestine; ULI = upper large intestine.

calculated from rats to baboons is in the intestinal absorbed doses. Rodents show excretion patterns significantly different from those of primates, and this fact is indicated by the data.

### Patient Imaging Studies

The clinical and pathologic features of the eight patients are outlined in Table 2. All patients had histologically proven neuroendocrine tumors. Five patients had proven carcinoid tumors of the gastrointestinal tract, and three had pancreatic islet cell tumors.

Abnormal foci of increased  $^{64}\text{Cu}$ -TETA-OC and  $^{111}\text{In}$ -DTPA-OC accumulation were seen in seven of the eight patients. These foci of increased activity were detected in several locations: small or large bowel (three patients), stomach (one patient), liver (four patients), pancreas (two patients), skin (one patient), abdominal and pelvic nodes (four patients), lung (one patient), and bone (two patients). The results of  $^{64}\text{Cu}$ -TETA-OC PET were, in general, similar to those of  $^{111}\text{In}$ -DTPA-OC and conventional scintigraphy (Figs. 1 and 2). One patient (patient 6, Fig. 2) showed osseous involvement in addition to the small-bowel lesions on  $^{64}\text{Cu}$ -TETA-OC PET. In two patients, more than one lesion was observed in the small bowel and bone with both agents (patients 2 and 6), and  $^{64}\text{Cu}$ -TETA-OC PET detected more lesions than did  $^{111}\text{In}$ -DTPA-OC imaging (Figs. 1 and 2). Although image contrast was better on  $^{64}\text{Cu}$ -TETA-OC PET, in some cases the image quality was better with  $^{111}\text{In}$ -DTPA-OC because of absence of intense activity in the kidneys and bladder.  $^{64}\text{Cu}$ -TETA-OC PET was falsely negative in a patient with a lung lesion, which showed uptake on the  $^{111}\text{In}$ -DTPA-OC scan. Disease seen with

$^{64}\text{Cu}$ -TETA-OC PET and  $^{111}\text{In}$ -DTPA-OC conventional scintigraphy was confirmed by a combination of histologic, radiologic, and clinical follow-up of the patients.

Mild to moderate blood-pool activity was present on images obtained immediately after tracer administration, with only faint blood-pool activity seen thereafter. Adrenal glands were visualized in three of eight patients (patients 1, 2, and 7) with  $^{64}\text{Cu}$ -TETA-OC PET. SSRs have been reported to be present in normal human adrenal glands as well as in malignant pheochromocytomas (14). No activity was seen in the gallbladder. Bowel activity was not present on early images but appeared faintly after 2 h and became more intense (mild to moderate) at 21–24 h after injection. Hepatic uptake was less than splenic uptake on the early images and became more intense with time, with the liver exhibiting activity similar to that in the spleen on delayed images. The renal collecting systems and bladder had high uptake at early times but became less intense on delayed images. Lesions were more clearly visualized on the early images than on the delayed images. The best imaging time appeared to be approximately 4–6 h after tracer injection.

### Pharmacokinetic Analysis

Blood samples were obtained from patients during their imaging sessions.  $^{64}\text{Cu}$ -TETA-OC cleared rapidly from the blood. The amount in the blood varied from patient to patient; however, by 4 h after injection,  $7.9 \pm 3.7$  %ID remained (range, 3.2–13.5 %ID). From 6 to 22 h after injection, the activity in the blood decreased further, with the amount in the blood ranging from 0.8 to 6.6 %ID (mean,  $3.3 \pm 2.3$  %ID). The large differences in blood-pool data are most likely related to patient-to-patient variation, pos-

**TABLE 2**  
Clinical, Imaging, and Histopathologic Patient Data

Patient no.	Age (y)	Sex	Tumor type	No. of lesions/sites		
				$^{111}\text{In}$ -DTPA-OC	$^{64}\text{Cu}$ -TETA-OC	Follow-up*
1	70	M	Carcinoid	6/SB and LN	6/SB and LN, adrenal glands	Multifocal/SB, 10/LN
2	45	M	Carcinoid	Innumerable/skin, stomach, pancreas, liver	Innumerable/skin, stomach, pancreas, liver, adrenal glands	Widespread disease
3	45	F	Carcinoid	1/LN, 3/bone, diffuse/liver	1/LN, 4/bone, LN, diffuse/liver	1/LN, diffuse/bone and liver
4	46	F	Islet cell NF pancreatic	No lesions	No lesions	No lesions
5	46	M	Islet cell MEN-I NF pancreatic	2/pancreas, 1/liver	2/pancreas, 1/liver	Multifocal/pancreas and spleen, 1/liver
6	58	M	Carcinoid	2/SB or LN	9/SB or LN, 2/bones	Multifocal/SB, 11/LN
7	61	M	Carcinoid	1/liver, 1/LN or SB	1/liver, 1/LN or SB, adrenal glands	1/liver, multiple/SB and LN
8	64	M	Islet cell NF pancreatic	1/lung, mild uptake	No lesions†	Numerous/liver, bone, pancreas, peritoneum

\*Pathologic, radiologic, and clinical.

†This patient did not undergo late imaging.

SB = small bowel; LN = lymph nodes; NF = nonfunctioning; MEN-I = multiple endocrine neoplasia, type I.



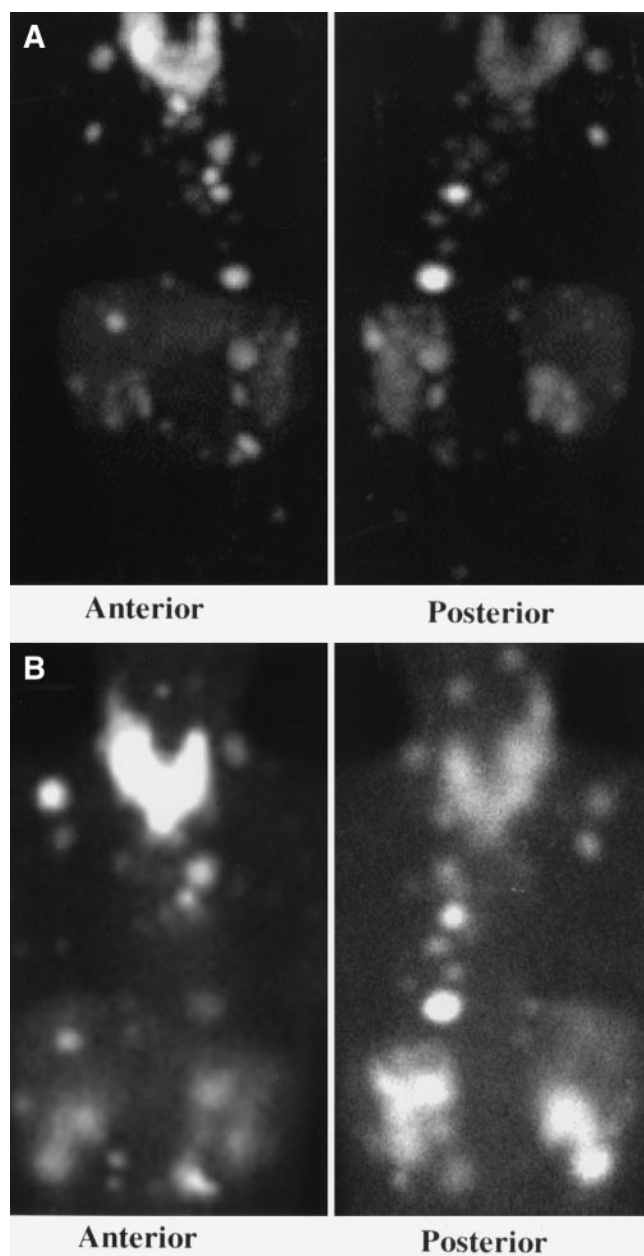


**FIGURE 1.** Anterior and posterior volume-rendered maximum pixel activity reprojected images of <sup>64</sup>Cu-TETA-OC PET (A) vs. anterior and posterior planar images of <sup>111</sup>In-DTPA-OC (B) throughout neck, chest, and abdomen of patient 2, 45-y-old man with numerous metastatic foci of carcinoid tumor. Images were obtained 4 h after injection.

sibly because of differing tumor burden. Urine excretion also varied between patients. During the first 4 h after injection, the amount excreted in the urine was  $44.6 \pm 10.6$  %ID, and the amount during 27 h was  $63.7 \pm 18.6$  %ID.

#### Human Dosimetry from Patient PET

Using PET data from five patients, the absorbed doses of <sup>64</sup>Cu-TETA-OC to the normal organs were measured. Time-activity curves are shown in Figure 3. Residence times were determined for seven tissues in which most of

the <sup>64</sup>Cu activity was localized, and they are listed in Table 3. From these data, the absorbed doses listed in Table 1 were determined. Residence times measured in the organs listed in Table 3 account for 35% of the maximum residence time, whereas 47% of activity was excreted in the urine. As predicted from the estimated absorbed doses from the rodent and baboon PET data, the human PET data indicate that the bladder wall is the dose-limiting organ, with an absorbed dose of 0.25 mGy/MBq (0.94 rad/mCi). This dose was calculated assuming emptying of the bladder at 4 h after injection. Other organs with higher absorbed doses include the liver (0.092 mGy/MBq [0.34 rad/mCi]), kidneys (0.078 mGy/MBq [0.29 rad/mCi]), and spleen (0.070 mGy/MBq [0.26 rad/mCi]). The intestinal dose was relatively low, as was the dose to the bone marrow.

#### DISCUSSION

The primary objective of this study was to determine the feasibility of PET imaging of neuroendocrine tumors in humans with <sup>64</sup>Cu-TETA-OC. <sup>64</sup>Cu-TETA-OC PET revealed tumors comparably with <sup>111</sup>In-DTPA-OC SPECT in six patients. Neither method detected tumors in patient 4; however, follow-up by CT did not reveal any tumors. The PET agent detected a larger number of lesions in two patients but did not detect a lung metastasis that showed mild uptake with <sup>111</sup>In-DTPA-OC SPECT in patient 8. Although the <sup>64</sup>Cu-TETA-OC PET images in patient 8 did not show the lung lesion, we were unable to obtain a delayed image for this patient, which may have shown the lesion. Figures 1 and 2 show images of patients 2 and 6, in whom more lesions were seen with <sup>64</sup>Cu-TETA-OC PET than with conventional imaging and SPECT with <sup>111</sup>In-DTPA-OC. Patient 2, whose images are shown in Figure 1, had numerous metastatic foci of a carcinoid tumor throughout his body. Especially extensive lymphadenopathy was present in the neck, and numerous lesions were in the liver, mediastinum, and bone. The <sup>64</sup>Cu-TETA-OC PET images revealed some of the smaller lesions, especially hepatic metastases, better than did the <sup>111</sup>In-DTPA-OC images. The reason may be either the better tumor-to-nontumor ratios for <sup>64</sup>Cu-TETA-OC or the better spatial resolution of PET compared with planar scintigraphy. In patient 6, carcinoid tumors in the abdomen were shown by both imaging methods. However, with <sup>64</sup>Cu-TETA-OC PET, osseous lesions were apparent that were not seen in the <sup>111</sup>In-DTPA-OC planar or SPECT images.

Urinary excretion of <sup>111</sup>In-DTPA-OC has been reported by several investigators (3,15,16). Although the reports vary, generally the total excretion during 24 h ranged from 65 to 85 %ID. In a study of 10 patients, Krenning et al. (3) reported a mean cumulative urinary excretion of 25 %ID at 3 h, 50 %ID at 6 h, and 85 %ID at 24 h. The cumulative urinary excretion of <sup>64</sup>Cu-TETA-OC was similar to that of <sup>111</sup>In-DTPA-OC, for which excretion was  $26.0 \pm 12.3$  %ID at 2 h,  $44.6 \pm 10.6$  %ID at 4 h, and  $63.7 \pm 18.6$  %ID at 27 h

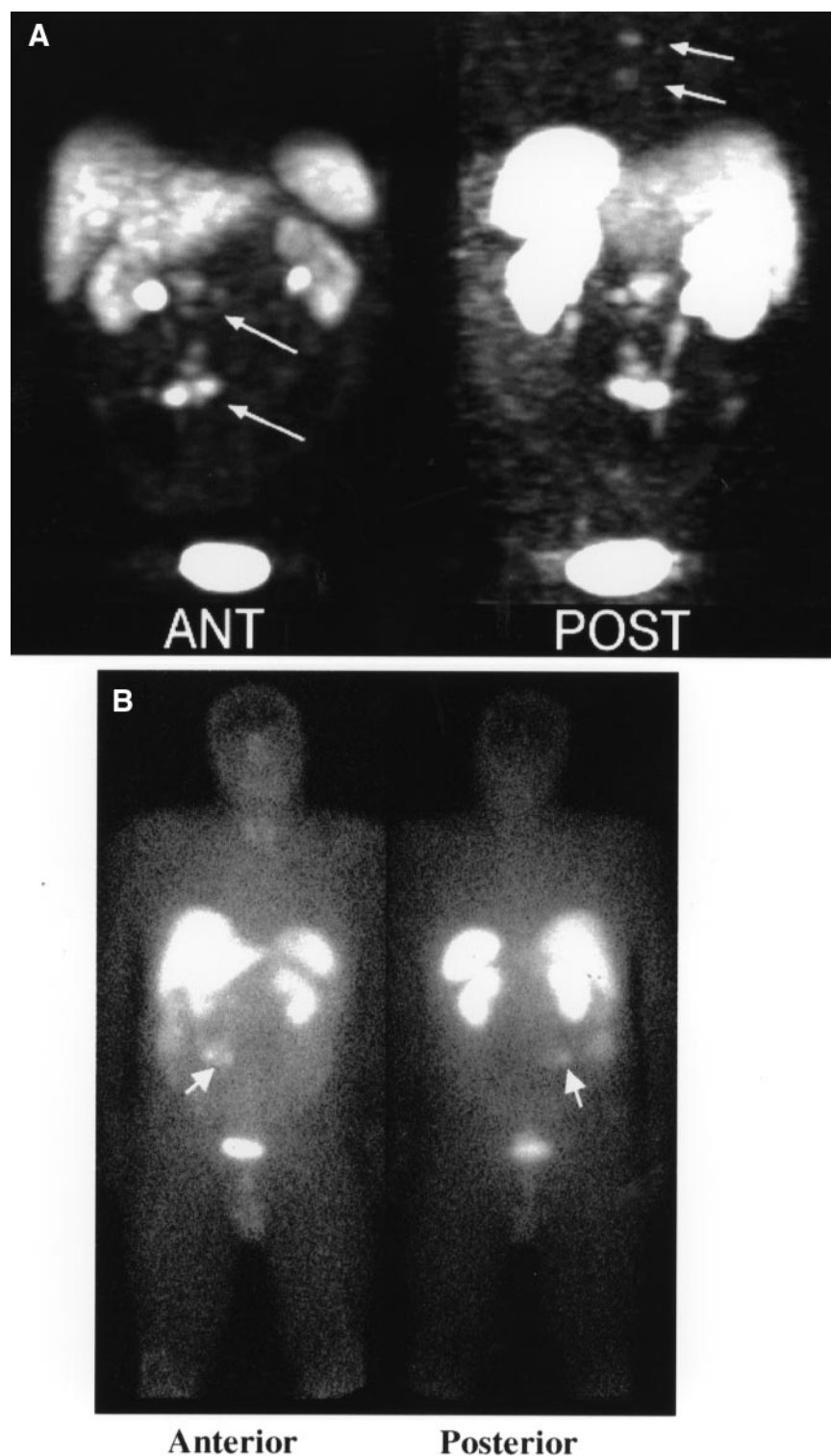


**FIGURE 2.** Anterior and posterior volume-rendered maximum pixel activity reprojected neck, chest, and abdomen images of  $^{64}\text{Cu}$ -TETA-OC PET (A) vs. anterior and posterior whole-body planar images of  $^{111}\text{In}$ -DTPA-OC (B) of patient 6, both obtained at 4 h after injection. Arrows in anterior image of (A) show abdominal carcinoid lesions, whereas posterior view of (A) shows osseous lesions. Arrows in anterior and posterior views of (B) indicate abdominal carcinoid tumors.

after injection. A few patients had an extensive tumor burden, and they excreted less  $^{64}\text{Cu}$ -TETA-OC.

Blood clearance of  $^{64}\text{Cu}$ -TETA-OC was similar to that of  $^{111}\text{In}$ -DTPA-OC at the earlier times; however,  $^{111}\text{In}$ -DTPA-OC cleared to a greater extent from the blood at later times. In a comparison study between  $^{111}\text{In}$ -DTPA-OC and  $^{111}\text{In}$ -

DOTA-Tyr<sup>3</sup>-OC, both agents showed approximately 10 %ID in the blood at 2 h after injection, with approximately 1 %ID remaining at 24 h (16). We observed approximately 8 %ID at 4 h, with clearance to approximately 3 %ID at 22 h after injection. The retention of  $^{64}\text{Cu}$  in the blood was not entirely surprising, because we found that in rats,  $^{64}\text{Cu}$ -

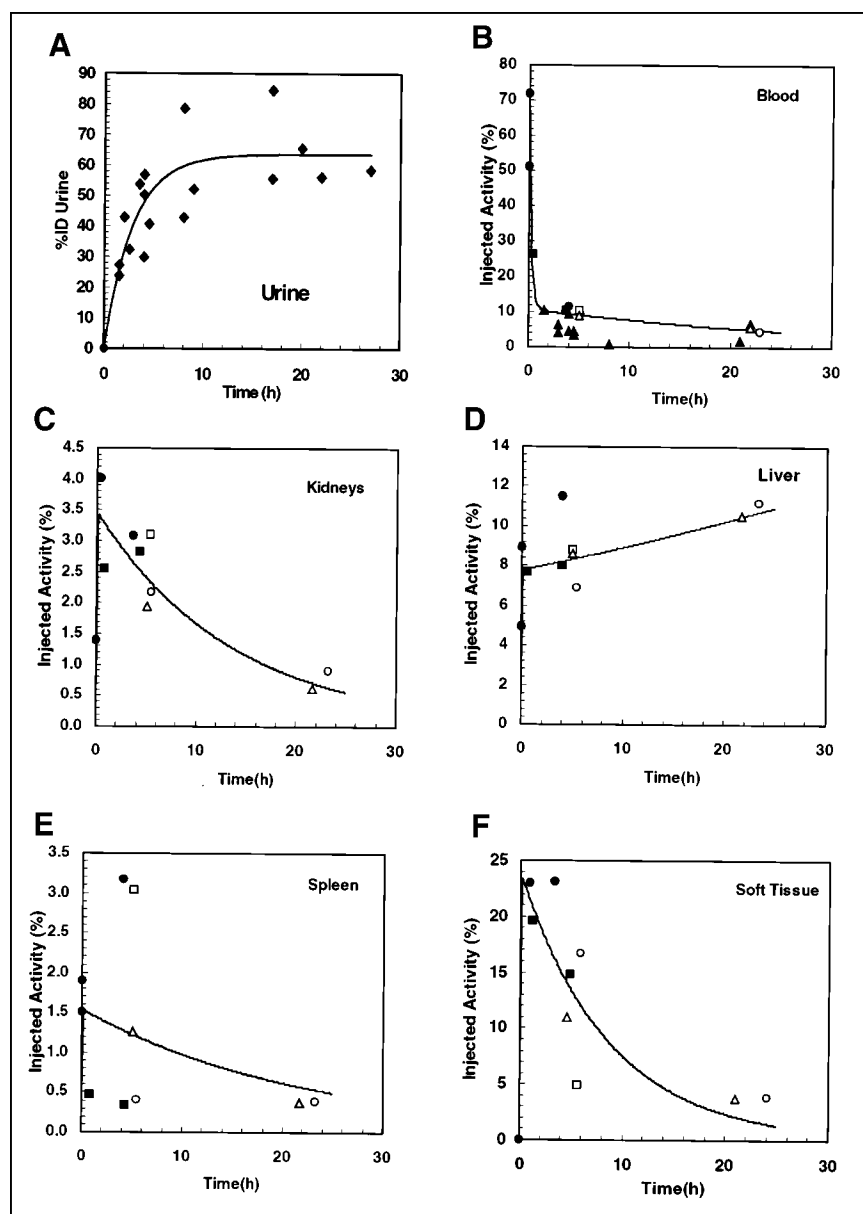


**FIGURE 3.** Cumulated patient time-activity curves. Unless noted, all values were determined from PET imaging data. (A) Urine data fitted with uptake function (percentage injected activity [%IA] =  $A_t (1 - \exp(-F_{ht} \times t))$ ,  $A_t = 63.6$ ,  $F_{ht} = 0.35$ ). These parameters were used in MIRDOSE3.0 bladder model with voiding period of 4 h to obtain average residence time of bladder contents. Urine data presented here were collected from all eight patients, and individual patient data are not indicated. (B–F) Data for blood clearance (B), kidney uptake (C), liver uptake (D), spleen uptake (E), and soft-tissue uptake (F).  $\blacktriangle$  = values determined from PET data;  $\bullet$  = patient 1;  $\circ$  = patient 2;  $\blacksquare$  = patient 6;  $\square$  = patient 7; and  $\triangle$  = patient 8.

TETA-OC also did not completely clear from the circulation (8). Recently, using a superoxide dismutase-specific assay, we showed that in rat liver,  $^{64}\text{Cu}$  dissociates from  $^{64}\text{Cu}$ -TETA-OC and binds to superoxide dismutase (17). Mirick et al. (18) reported that  $^{67}\text{Cu}$ -BAT-2IT-Lym-1 (where BAT = 6-[p-(bromoacetamido)benzyl]-1,4,8,11-tetraazacyclotetradecane- $N,N',N'',N'''$ -tetraacetic acid and 2IT = 2-iminothiolane) dissociated and that  $^{67}\text{Cu}$  bound to ceruloplasmin, causing retention of  $^{67}\text{Cu}$  in the blood. In the patients administered  $^{64}\text{Cu}$ -TETA-OC, some dissociation of  $^{64}\text{Cu}$  likely occurred, with subsequent binding to plasma proteins. Future patient PET imaging studies will include metabolite analyses of blood and urine.

A preliminary evaluation of absorbed doses in normal organs, performed by averaging PET data from five patients, showed that the urinary bladder was the dose-limiting

**TABLE 3**  
Organ Residence Times in Humans for  $^{64}\text{Cu}$ -TETA-OC from PET Images

Tissue	Residence time (h)	Error ( $\pm$ )
Liver	1.90	0.29
Kidneys	0.27	0.04
Spleen	0.15	0.04
Blood	1.35	0.09
Bone marrow	0.09	0.01
Soft tissue	1.39	0.14
Bladder content*	1.27	

\*Bladder content was calculated from bladder model in MIRDOSE3 (12).

organ (0.25 mGy/MBq [0.94 rad/mCi]). This finding was predicted from human absorbed dose measurements estimated from rat biodistribution and baboon PET imaging data. The dose to the urinary bladder using baboon PET imaging data and human PET data was determined using the MIRDOSE3 bladder model (12) along with a voiding period of 4 h to obtain the residence time of the bladder contents. If patients were to be given intravenous fluids or asked to drink large quantities of fluids, the voiding time could be decreased to 1 h, which would reduce the absorbed dose to 0.062 mGy/MBq (0.23 rad/mCi). The liver would then be the dose-limiting organ (0.091 mGy/MBq [0.34 rad/mCi]).

Although the human absorbed dose estimates from rats, nonhuman primates, and humans indicate the bladder wall to be the dose-limiting organ, significant differences are seen when different species are used to estimate dosimetry. The use of rodent biodistribution data is generally thought to give a worst-case estimate of absorbed doses to normal organs; however, the data in Table 1 suggest that the use of rat biodistribution data underestimates the dose to the liver and spleen. As shown in Figure 3D, the percentage injected activity of  $^{64}\text{Cu}$ -TETA-OC in the liver increases over time.  $^{64}\text{Cu}$  may dissociate from the TETA chelator in human liver to a greater extent than it does in rat or baboon liver, and this dissociation may be responsible for the higher absorbed dose. The human dosimetry data also show the spleen to have a considerably higher absorbed dose than was extrapolated from rodent and baboon data. One proposal is that somatostatin regulates immune function in humans and that, therefore, SSRs are present in the spleen (19). The cumulative time–activity curve for the spleen (Fig. 3E) shows that the data are highly variable among the different patients, and a large error is therefore associated with the absorbed dose value. The absorbed dose to the spleen from  $^{111}\text{In}$ -DTPA-OC measured in humans is consistent with our data obtained with  $^{64}\text{Cu}$ -TETA-OC and PET (15).

Overall, the normal-organ dosimetry suggests that PET imaging with 111 MBq (3 mCi)  $^{64}\text{Cu}$ -TETA-OC gave reasonable absorbed doses to normal organs, with the urinary bladder (the critical organ) receiving less than 20 mGy (3 rad). In future PET imaging studies, the administered dose will be raised to approximately 518 MBq (14 mCi) and the patients will be asked to drink large quantities of fluids and to void frequently. We anticipate that these changes will provide higher image quality with less than 50 mGy (5 rad) to the urinary bladder or liver.

## CONCLUSION

We evaluated  $^{64}\text{Cu}$ -TETA-OC as a potential PET tracer for imaging neuroendocrine tumors.  $^{64}\text{Cu}$ -TETA-OC PET compared well with  $^{111}\text{In}$ -DTPA-OC and conventional imaging, with more tumors being visualized in two patients. The blood clearance and urinary excretion of  $^{64}\text{Cu}$ -TETA-OC were similar to those of  $^{111}\text{In}$ -DTPA-OC at earlier times, but at later times  $^{111}\text{In}$ -DTPA-OC clearance from the blood

and excretion into the bladder were greater. The human absorbed doses to normal organs from  $^{64}\text{Cu}$ -TETA-OC were estimated using rodent biodistribution data, baboon PET imaging data, and human PET imaging data. The baboon PET data more accurately estimated the human dosimetry than did the rodent data; however, both methods underestimated the absorbed doses to the liver and spleen. Although  $^{64}\text{Cu}$ -TETA-OC has promise as a PET imaging agent for neuroendocrine tumors, our ultimate goal would be to use this agent for PET imaging before using this agent for targeted radiotherapy. Future studies include determining tumor dosimetry, which will provide information on the potential of  $^{64}\text{Cu}$ -TETA-OC for therapy.

## ACKNOWLEDGMENTS

The authors thank Dr. Michael J. Welch for providing  $^{64}\text{Cu}$ ; Diana Trask, Helen Kaemmerer, and John Englebach for excellent technical assistance; and Dr. Barry A. Siegel for helpful discussions. This study was supported by grant CA64475 from the National Institutes of Health, Bethesda, MD; a grant from Mallinckrodt, Inc.; and grant DE-FG02-96ER92216 from the Department of Energy.

## REFERENCES

- Bakker WH, Krenning EP, Breeman WA, et al. In vivo use of a radioiodinated somatostatin analogue: dynamics, metabolism, and binding to somatostatin receptor-positive tumors in man. *J Nucl Med.* 1991;32:1184–1189.
- Bakker WH, Krenning EP, Reubi JC, et al. In vivo application of [In-111-DTPA-D-Phe]-octreotide for detection of somatostatin receptor-positive tumors in rats. *Life Sci.* 1991;49:1593–1601.
- Krenning EP, Bakker WH, Kooij PPM, et al. Somatostatin receptor scintigraphy with indium-111-DTPA-D-Phe-1-octreotide in man: metabolism, dosimetry and comparison with iodine-123-Tyr-3-octreotide. *J Nucl Med.* 1992;33:652–658.
- Zinn KR, Chaudhuri TR, Cheng TP, Morris JS, Meyer WA. Production of no-carrier-added Cu-64 from zinc metal irradiated under boron shielding. *Cancer.* 1994;73:774–778.
- McCarthy DW, Shefer RE, Klinkowstein RE, et al. The efficient production of high specific activity Cu-64 using a biomedical cyclotron. *Nucl Med Biol.* 1997;24:35–43.
- Connett JM, Anderson CJ, Guo LW, et al. Radioimmunotherapy with a Cu-64-labeled monoclonal antibody: a comparison with Cu-67. *Proc Natl Acad Sci USA.* 1996;93:6814–6818.
- Connett JM, Buettner TL, Anderson CJ. Maximum tolerated dose and large tumor radioimmunotherapy studies of  $^{64}\text{Cu}$ -labeled MAb 1A3 in a colon cancer model. *Clin Cancer Res.* 1999;5(suppl):3207s–3212s.
- Anderson CJ, Pajean TS, Edwards WB, Sherman ELC, Rogers BE, Welch MJ. In vitro and in vivo evaluation of copper-64-labeled octreotide conjugates. *J Nucl Med.* 1995;36:2315–2325.
- Anderson CJ, Jones LA, Bass LA, et al. Radiotherapy, toxicity and dosimetry of copper-64-TETA-octreotide in tumor-bearing rats. *J Nucl Med.* 1998;39:1944–1951.
- Xu M, Cutler PD, Luk WK. An adaptive local threshold segmented attenuation correction method for whole-body PET imaging. *IEEE Trans Nucl Sci.* 1996;43:331–336.
- Siegel JA, Pawlyk DA, Lee RE, et al. Tumor, red marrow, and organ dosimetry for I-131-labeled anti-carcinoembryonic antigen monoclonal antibody. *Cancer Res.* 1990;50:1039s–1042s.
- Stabin MG. MIRDOSE: personal computer software for internal dose assessment in nuclear medicine. *J Nucl Med.* 1996;37:538–546.
- Lewis JS, Lewis MR, Cutler PD, et al. Radiotherapy and dosimetry of  $^{64}\text{Cu}$ -TETA-Tyr<sup>3</sup>-octreotate in a somatostatin receptor-positive tumor-bearing rat model. *Clin Cancer Res.* 1999;5:3608–3616.
- Epelbaum J, Bertherat J, Prevost G, et al. Molecular and pharmacological



- characterization of somatostatin receptor subtypes in adrenal, extraadrenal, and malignant pheochromocytomas. *J Clin Endocrinol Metab.* 1995;80:1837–1844.
15. Stabin MG, Kooij PPM, Bakker WH, et al. Radiation dosimetry for In-111-pentetreotide. *J Nucl Med.* 1997;38:1919–1922.
16. Kwekkeboom DJ, Kooij PP, Bakker WH, Maecke HR, Krenning EP. Comparison of <sup>111</sup>In-DOTA-Tyr<sup>3</sup>-octreotide and <sup>111</sup>In-DTPA-octreotide in the same patients: biodistribution, kinetics, organ and tumor uptake. *J Nucl Med.* 1999;40:762–767.
17. Bass LA, Wang M, Welch MJ, Anderson CJ. In vivo transchelation of copper-64 from TETA-octreotide to superoxide dismutase in rat liver. *Bioconjug Chem.* 2000;11:527–532.
18. Mirick GR, O'Donnell RT, DeNardo SJ, Shen S, Meares CF, DeNardo GL. Transfer of copper from a chelated <sup>67</sup>Cu-antibody conjugate to ceruloplasmin in lymphoma patients. *Nucl Med Biol.* 1999;26:841–845.
19. Reubi JC, Waser B, Horisberger U, et al. In vitro autoradiographic and in vivo scintigraphic localization of somatostatin receptors in human lymphatic tissue. *Blood.* 1993;82:2143–2151.



The Journal of  
NUCLEAR MEDICINE

## **$^{64}\text{Cu}$ -TETA-Octreotide as a PET Imaging Agent for Patients with Neuroendocrine Tumors**

Carolyn J. Anderson, Farrokh Dehdashti, P. Duffy Cutler, Sally W. Schwarz, Richard Laforest, Laura A. Bass, Jason S. Lewis and Deborah W. McCarthy

*J Nucl Med.* 2001;42:213-221.

---

This article and updated information are available at:  
<http://jnm.snmjournals.org/content/42/2/213>


---

Information about reproducing figures, tables, or other portions of this article can be found online at:  
<http://jnm.snmjournals.org/site/misc/permission.xhtml>

Information about subscriptions to JNM can be found at:  
<http://jnm.snmjournals.org/site/subscriptions/online.xhtml>

*The Journal of Nuclear Medicine* is published monthly.  
SNMMI | Society of Nuclear Medicine and Molecular Imaging  
1850 Samuel Morse Drive, Reston, VA 20190.  
(Print ISSN: 0161-5505, Online ISSN: 2159-662X)

© Copyright 2001 SNMMI; all rights reserved.

 SOCIETY OF  
NUCLEAR MEDICINE  
AND MOLECULAR IMAGING